J Mater Sci (2016) 51:1000–1016
DOI 10.1007/s10853-015-9431-0

Proton-radiation resistance of poly(ethylene terephthalate)–nanodiamond–graphene nanoplatelet nanocomposites

V. Borjanović[1,2] · L. Bistričić[1] · I. Pucić[3] · L. Mikac[3] · R. Slunjski[3] · M. Jakšić[3] · G. McGuire[2] · A. Tomas Stanković[4] · O. Shenderova[2]

Received: 20 May 2015 / Accepted: 9 September 2015 / Published online: 21 September 2015

Abstract Poly(ethylene terephthalate) nanocomposites reinforced with 1 wt% of nanodiamond terminated with carboxylic groups or nanodiamond and 0.3 wt% nanographene platelets were prepared by simple melt blending in a twin-screw extruder to create high-performance polymer nanocomposites for application in high radiation environments. A study of structural modifications introduced by high-energy, 3 MeV proton beam irradiation of poly(ethylene terephthalate) and its nanocomposites was conducted using attenuated total reflectance Fourier transform infrared and Raman spectroscopy, differential scanning calorimetry, and photoluminescence measurements. It was shown that the composite materials containing small concentrations of nanodiamonds or nanodiamonds plus nanographene platelets exhibit improved radiation resistance compared with neat poly(ethylene terephthalate) exposed to proton irradiation under the same irradiation conditions. The nanocomposites containing the combination of nanodiamonds and nanographene platelets exhibited the highest stability. Nanofillers, particularly nanographene platelets, stabilized the amorphous phase and increased the crystallinity of polymer matrix exposed to proton irradiation, preserving polymer conformation, molecular weight distribution, and overall thermal properties of irradiated nanocomposites.

✉ V. Borjanović
vesna.borjanovic@fer.hr

[1] Faculty of Electrical Engineering and Computing, University of Zagreb, Unska 3, 10000 Zagreb, Croatia

[2] International Technology Center, 8100-120 Brownleigh Dr., Raleigh, NC 27617, USA

[3] Ruđer Bošković Institute, Bijenička 54, Zagreb, Croatia

[4] Energy Institute Hrvoje Požar, Savska cesta 163, Zagreb, Croatia

Introduction

Poly(ethylene terephthalate) (PET) films have attracted major industrial interest due to their ample range of applications, low cost, and wide availability. PET has good mechanical properties, chemical resistance, thermal stability, high transparency and flexibility, light weight, low gas permeability (especially to oxygen, carbon dioxide, and water vapor), and the ability to be spun in the form of fibers [1]. Therefore, it is commonly used in packaging and fiber applications (beverage bottles, textiles, engineering plastics in automobiles, etc.), as well as in the electronics industry (electric parts, transparent substrates for flexible electric devices such as organic light-emitting diodes (OLED's), solar cells, etc.), and the biomedical industry (human implants such as vascular grafts, prosthetic heart valves, and for endothelial cell growth) [2, 3]. PET is a thermoplastic, long chain polymer. It is either in the amorphous state or semi-crystalline state, which means it consists of amorphous and crystalline phases. Its properties depend mainly on the degree of orientation of the polymer chains as well as the level of crystallinity. The extent of crystallinity of PET depends on its process and thermal history. Polymers with a high degree of crystallinity have a higher glass transition temperature, T_g, higher modulus, toughness, stiffness, tensile strength, and hardness, and are more resistant to solvents, but have lower impact strength [4, 5].

Compounding of polymers with different fillers is a common and versatile approach to acquiring new desirable properties at a favorable cost/performance ratio. Conventional fillers have been used to improve polymer properties

(e.g., decreasing oxygen permeability in food packaging, increasing flame resistance in textiles, increasing the modulus in injection molded parts, etc.) and to reduce cost. However, there are limitations in their application due to phase separation, particle agglomeration, and heterogeneous distribution of the filler in the product [6]. Polymer nanocomposites are mixtures of polymer and nanometer-length-scale particles, whereas, conventional polymer composites contain micrometer scale particles. Polymer nanocomposites have attracted a great deal of interest in the scientific and industrial fields because of the remarkable improvements achieved in their physical and mechanical properties at very low filler loadings [7–9]. The introduction of various kinds of additives is performed to adjust polymer properties for specific applications. Due to the extensive and still-growing use of polymeric materials for the variety of technological applications listed above, the study of the stability and stabilization of polymers under irradiation has become an important issue. Knowledge of the filler's influence on the polymer's properties under irradiation, however, remains limited. Radiation-resistant polymers can be advantageously used in the manufacture of scintillators, medical devices, and structures used in space or any other high irradiation environment.

There have been numerous reports on radiation-induced modifications of PET. The studies on the effects of irradiation by various energetic ions on the physical properties of PET have been reported by Mishra et al. [10], Bridwell et al. [11], Keiji et al. [12], Singh et al. [13, 14], Fink et al. [15], etc. They studied its modified physical–chemical properties by exposing it to swift photo ions of protons as well as swift heavy ions as varied as helium, lithium, boron, carbon, nitrogen, silicon, etc. According to the study by Singh et al. on the modification of PET by proton irradiation [14], there is no significant change in the stability of the polymer up to the fluence of 10^{14} ions cm^{-2}. FTIR spectra indicated that PET was chemically degraded at the highest proton fluence used in their study, i.e., 10^{15} ions cm^{-2}. Furthermore, Singh et al. also studied the electric and thermal behaviors of proton-irradiated polymeric blends [14].

The use of PET under severe conditions requires that its various physical properties, such as optical, thermal, mechanical, and barrier properties, should be enhanced. Hence, considerable effort has been devoted to improving the various physical properties of PET through mixing it with different nanofillers, both organic and inorganic [16].

Carbon nanotubes (CNTs) have been the most explored carbon-based nanomaterial used as a filler material in a PET matrix. Kim et al., Tzavalas et al., and Liu and Kumar studied crystallization behavior, mechanical properties, thermal behavior, etc., of PET-multiwall carbon nanotube (MWCNT) nanocomposites [17–19]. Wang et al. studied polymers containing fullerenes or carbon nanotube structures [20].

This is for the first time to the best of our knowledge that nanodiamond (ND) and nanographene platelets (NGPs) have been introduced as fillers in the PET polymer matrix with the goal of achieving higher proton radiation resistance.

Nanodiamond, produced by detonation (DND) synthesis in large volumes is a relatively inexpensive carbon nanomaterial for a broad range of potential applications, including composites [21]. Superior hardness and thermal conductivity of the diamond core is combined in nanodiamond powders with large accessible surface area covered by readily tailorable surface functional groups.

In our previous works [22–25], it was shown that nanodiamond–polydimethylsiloxane (ND–PDMS)-based nanocomposite materials exhibit enhanced stability against high-energy proton irradiation compared to pure PDMS [25]. The appearance of strong photoluminescence (PL) following irradiation, more pronounced for PDMS–DND composites compared to pure PDMS, was reported. The findings suggested the broad application of polymer composites containing ND particles in spacecraft materials, such as the material for irradiation-dose determination for spacecraft or aircraft flying at high altitudes through changes in the PL intensity.

Graphene is particularly valuable because it has exceptional electric, mechanical, thermal, optical, and barrier properties. Improvements in mechanical and electric properties of polymer composites of graphene are much greater than those of composites of clay or other carbon-based fillers [9, 26]. Although carbon nanotubes (CNTs) and graphene show comparable mechanical properties, graphene is reported to be a better nanofiller than CNT in terms of certain aspects such as thermal and electric conductivities [27]. Zhang et al. prepared PET/graphene nanocomposites by melt mixing with the aim of characterizing their gas permeability and mechanical properties. It was reported that PET composite films containing 2 wt% of a few graphene layers showed more than 70 % decrease in N_2 gas permeation and 10–21 % increase in modulus, [28].

In this work, we introduced NGP, with multifunctional properties into a PET matrix forming a PET–ND–NGP composite to further enhance thermal conductivity and thermo-oxidative resistance of the resulting composite material. As our intention was to keep the electric properties of the nanocomposite the same as the neat PET, we introduced just a small percentage of NGPs into the PET matrix (0.3 wt%) combined with highly dielectric NDs. A ND loading of 1 wt% was chosen since it is a concentration where the best mechanical\thermal properties were achieved for ND composites in many previous works

(including ours). At higher concentrations, aggregates are formed which cause degradation of the composites properties. In the ND\NGP composite, one goal was to determine if there are any synergistic benefits as has been reported previously [29].

Processability of composites is a key consideration (not raising the viscosity of the composites to too high values and avoiding agglomeration of the nanoadditives). It is also known that sub-1 wt% of nanographene provides noticeable improvements in the properties. Thus, based on the previous works where mechanical\thermal properties are improved and nanoadditives were relatively well dispersed, we chose 1 wt% of ND and 0.3 wt% of NGP.

In this article, we present a study of structural modifications introduced by high-energy, 3 MeV, proton beam irradiation of PET- and PET-carbon-based nanocomposites. We show using attenuated total reflectance Fourier transform infrared (ATR-FTIR), Raman, differential scanning calorimetry (DSC), and photoluminescence (PL) measurements that the composite materials, PET–ND and PET–ND–NGP, exhibit improved radiation resistance compared with pure PET exposed to proton irradiation under the same irradiation conditions.

Materials and methods

PET–nanodiamond (PET–ND) and PET–nanodiamond–graphene nanoplatelet (PET–ND–NGP) composites fabrication

Commercially available PET (Polyclear 1101 q, IV, intrinsic viscosity 0.83 dL g^{-1}) from Indorama Ventures, and carbon-based nanocomposites of the PET were melt-cast using a twin screw extruder at the North Carolina Polymer Center of Excellence to a thickness of about 150 μm. The as-received PET was in the form of pellets on the order of a few mm in diameter. The pellets were reduced by grinding to a powder. The nanomaterials were introduced into the powder, and the mixture was subjected to further grinding/mixing. The nanofiller containing PET powder underwent additional mixing in the twin screw extruder under shear above the softening temperature of the polymer. This method has several advantages over other methods: this method does not require a solvent. A suitable solvent in which to disperse the nanoparticles which is also a solvent to PET is difficult to identify. The residence time at high temperature during extrusion is shorter than that in the case of in situ polymerization. This approach could be used for the production and processing techniques implemented on commercial scale.

Nanodiamond used in this study was prepared as previously reported [21]. For this study, NDs with ~100-nm particle size with a large fraction of 30-nm particles terminated with carboxylic groups was prepared. The introduction of carboxylic groups on the surface of the nanoparticle as a result of acid treatment leads to enhanced interaction between the NDs and the polymer matrix through hydrogen bonding. The thermal stability, mechanical, and rheorogical properties of PET nanocompoistes are dependent on the interfacial interactions between the PET and the functionalized ND as well as the dispersion of the nanoparticles.

The functionalized ND may also help in the dispersion of NGP by reducing the π–π stacking among the aromatic rings of the graphene nanoplatelets, which leads to the formation of the aggregates. The NGPs were purchased from Angstrom Materials (product number N006-010-P). The NGPs have average x and y dimensions of 14 μm and z dimension of 10–20 nm.

Proton irradiation conditions

Samples of pure PET, PET–ND, and PET–ND–NGP nanocomposites were irradiated in vacuum by means of a 3-MeV proton beam that was delivered by the 1.0 MV Tandetron accelerator at the Ruđer Bošković Institute, Zagreb, Croatia. A homogeneous circular beam of 5 mm in diameter was used. Irradiations with a 40-nA proton beam current were carried out for all samples. Samples of PET and PET nanocomposites were irradiated in three areas with different fluences ranging from 10^{14} protons cm^{-2} to 10^{16} protons cm^{-2}. The fluence corresponding to region 1 (*D1*) is 10^{14} p cm^{-2}, that to region 2 (*D2*) is 10^{15} p cm^{-2}; and that to region 3 (*D3*) is 10^{16} p cm^{-2}. All irradiations were performed at the room temperature.

Characterization of pristine and irradiated films

The characteristics of the proton beam-induced changes in pristine PET and PET nanocomposites were analyzed using ATR-FTIR and Raman spectroscopy, DSC, and PL measurements. The ATR-FTIR spectra were recorded using an ABB Bomem MB 102 spectrometer. The spectra of pure PET as well as PET–ND and PET–ND–NGP nanocomposites were recorded over the frequency range of 600–3200 cm^{-1} using Specac's Golden Gate Single Reflection Diamond ATR System with a ZnSe lens. The spectra were collected with a resolution of 2 cm^{-1} by combining the results of 10 scans. A reference spectrum was collected before each measurement.

Raman spectra were recorded on a Horiba Jobin–Yvon T64000 instrument equipped with the Olympus open microscope stage and CCD Symphony detector. The spectrometer was operating in the triple subtractive mode during the acquisition of spectra. The 514.5-nm line of a

Coherent INNOVA-400 argon ion laser was used for excitation. Spectra were recorded from 50 to 3100 cm^{-1}. The laser power used to measure the Raman spectra was 20 mW at the sample.

For the DSC measurements, ~2 mg sample films were used. In the case of irradiated samples, regions were cut out from each film in such a way as to ensure the highest possible homogeneity. Samples were put in Al pans and their thermograms recorded in a nitrogen atmosphere on a Perkin-Elmer Pyris Diamond DSC instrument. Two heating–cooling cycles were performed for each sample in the temperature range of 50–300 °C, at a rate of 20 °C min^{-1}.

The PL spectra of the samples were recorded at room temperature on a GWTech diffraction grating spectrometer, using a 405-nm diode laser (the laser power was 0.5 mW). The laser beam was focused to a 30–40-μm diameter. The acquisition times of the PL spectra were the same for all samples (150 ms).

Results and discussion

FTIR analysis

Pristine nanodiamond and graphene nanocomposites

FTIR spectroscopy is one of the most powerful among the qualitative and quantitative methods applied for studying molecular bonding and functional group analysis. The vibrational bands in the FTIR spectra of PET give dual information. First, every peak position is fundamental to the molecular bonding or existing functional groups. Therefore, any shift in peak position in a spectrum directly reflects a change in bond strength or bond angle. Such a change is highly probable in a complex structure as in the case of PET. This means any change in the network structure of PET directly influences some of the functional groups (=CO, –CHO, –OH, etc.) of the material. Such interactions either weakens or strengthens bonding which corresponds to a shift of the wave number of the corresponding absorption peak to lower or higher values, respectively. The absence of a particular molecular bond relates to scission of a particular bonding structure. Secondly, variation in intensity of a particular peak in a spectrum correlates primarily to the concentration of the corresponding functional group in the material. However, the intensity of some absorption peaks may also vary due to crystallization.

FTIR spectroscopy was used to examine and monitor the changes introduced by the incorporation of the carbon-based nanofillers into the PET polymer matrix as well as changes produced by different fluences of high-energy proton irradiation of neat PET and PET nanocomposites. To elucidate the structural effects of incorporating different carbon-based nanofillers into the PET matrix, FTIR spectra of pristine (nonirradiated) PET and pristine PET nanocomposites were acquired. The aim was to reveal possible interactions/changes in the PET matrix induced by the incorporation of ND or ND and NGP. Further, FTIR spectra of proton-irradiated samples were acquired and compared with the spectra of the unirradiated samples to gain insight into radiation-induced changes in PET and PET nanocomposites.

The spectrum of nanodiamond functionalized with carboxylic groups used in our study was reported and discussed previously [30]. Although the vibrational bands in the FTIR spectrum of pure PET have been reported previously [30–33], Table 1 presents the assignments of the bands according to the published literature again here for ease of comparison. The spectra of pure PET and PET nanocomposites are presented in Fig. 1 for comparison.

As it can be seen from Fig. 1 the FTIR spectra of pure PET, PET–ND, and PET–ND–NGP do not show any obvious differences in peak positions and intensities. Addition of ND and ND–NGP nanofillers did not significantly modify the shape of the vibrational spectra of the PET matrix and no new vibrational bands were detected. According to these results, the addition of nanofillers did not appear to significantly change the polymer matrix. For such a small concentration of nanoparticles, FTIR's sensitivity may not be high enough to identify hydrogen bonding between ND and the matrix material.

The *trans* conformation of oxygen atoms in the glycol segment (–O–CH_2–CH_2–O–) [34] and the *trans* planar conformation of the terephthalate groups are associated with PET crystallization. This combination presents a near linear arrangement of the polymer chain, permitting closer packing and development of crystalline regions. So in the crystalline phase, the ethylene glycol segment has a *trans* conformation with ordered terephthalate groups. The *gauche* glycol and *cis*-terephthalate (disordered terephthalate units) conformations lead to an amorphous structure. In most cases, though, the two structures seem to coexist within the amorphous part of a PET sample; a completely disordered amorphous structure and an "intermediate" amorphous structure [35]. Thus, PET is better described by a three phase model comprising: (a) crystalline phase constituted exclusively of the *trans* conformation (b) an "intermediate" phase consisting of the *trans* conformation that does not belong to the crystalline phase and some gauche conformation, and (c) a third completely disordered phase which contains mainly the *gauche* conformation. One of the well-documented methods for characterizing the chain conformation and crystallinity is the vibrational spectroscopy.

Table 1 Assignment of the vibrational bands in the spectrum of PET [31–33]

IR (cm^{-1})	Assignment
2956 vw	CH_2 stretching
2925 vw	CH_2 stretching
2852 vw	CH_2 stretching
1714 s	C=O stretching
1615 vw	C=C stretching (ring)
1578 vw	C–C stretching (ring)
1505 vw	C–C stretching (ring)
1455 vw	CH_2 scissoring
1443 vw	CH_2 scissoring
1410 w	C–C stretching (ring)
1370 vw	CH_2 wagging (*gauche*)
1340 vw	CH_2 wagging (*trans*)
1282 sh,m	C–C stretching (ring) and C–O stretching
1257 sh,m	C–C stretching (ring) and C–O stretching
1238 s	C–C stretching (ring) and C–O stretching
1175 w	CH in-plane bend (ring)
1116 m	CH in-plane bend (ring) and C–O stretching
1092 s	CH in-plane bend (ring) and C–O stretching
1041 w	C–C stretching (glycol)
1016 m	CH in-plane bend (ring)
973 vw	C–H out-of-plane bending
898 vw	CH_2 rocking
874 w	CH out-of-plane bend (ring)
841 vw	C–C stretching (ring breathing)
795 w	CH out-of-plane bend (ring)
723 s	CC in-plane bend (ring) and CH out-of-plane bend (ring)

s strong, *m* moderate, *w* weak, *v* very, *sh* shoulder

For PET, there are several infrared bands that can be linked to the polymer structure and orientation [35, 36]. These bands can be used to differentiate the *trans*- and *gauche*-rotational isomers of PET, which can further be correlated to polymer crystallinity. The crystallinity in PET is usually induced by thermal crystallization and/or by stress- or strain-induced crystallization [37]. For example, the absorption bands at 1042 and 898 cm^{-1} are indicative of the *gauche*- isomer and the 973 and 850 cm^{-1} bands are indicative of the *trans*- conformation [36]. The bands have been assigned to the ethylene glycol linkage, which is the O–CH_2–CH_2–O section within the polymer chain. Molecular orientation can be extracted from the 973 cm^{-1} band. Orientation-specific data can also be extracted from different chemical moieties within the polymer chain. The 874 cm^{-1} band, attributed to the C–H out-of-plane deformation of the benzene ring in the terephthalate group, is also sensitive to molecular orientation [35]. Thus, by using FTIR it is possible to identify bands characteristic of the amorphous and crystalline phase. Furthermore IR conformational bands can be used to follow the PET crystallization process as well as to assess the presence of a crystal phase in starting samples [38]. The usual method to quantitatively compare the crystal fraction in films, which was used in this study, is to compare the integrated intensities of the *trans*-glycol conformation band at 1340 cm^{-1} (I_{1340}) with the integrated intensity of a reference band that is unaffected by conformational changes of the monomeric unit. It can be used to normalize the spectral bands of PET [39]. The PET band at 1410 cm^{-1}, which is associated with the ring in—plane deformation, is assumed to be such a band. The absorption band at 1370 cm^{-1} represents the *gauche* conformation band.

So, to analyze the FTIR spectra we performed fitting of the vibrational bands in the frequency region 1300–1450 cm^{-1} to a Lorentz shape. The ratio of the integrated intensities I_{1340}/I_{1410} and I_{1372}/I_{1410} represent the fraction of the glycol segment in *trans* and *gauche* conformations, respectively, in pristine PET and PET nanocomposites. The results of the analysis for PET and PET nanocomposites are presented in Table 2 for both nonirradiated and irradiated samples for the sake of clarity

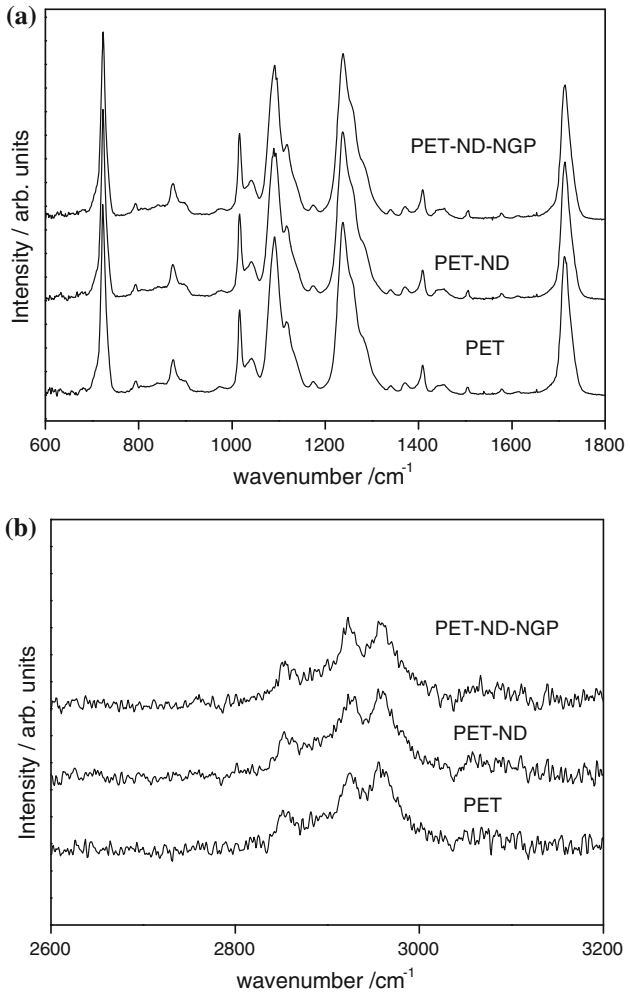

Fig. 1 FTIR spectra of unirradiated PET and PET nanocomposites. The spectra were recorded over the frequency range 600–3200 cm^{-1}

and ease of comparison. The analysis indicates a slightly higher fraction of the *trans* conformation in both nanocomposite materials (0.330 in PET versus 0.360 in PET–ND and PET–ND–NGP composites) with almost the same fraction of the *gauche* conformation in all the samples (see Table 2). However, analysis showed some small changes in *trans/gauche* fractions indicating that functionalized NDs probably interact with PET mainly via van der Waals interactions. The nanoparticles may serve as nucleating agents increasing (slightly) the crystalline phase content of the polymer matrix. But fast cooling during the material production did not allow the crystallization process to proceed as far as may be possible with a slower cooling rate.

Proton-irradiated PET and PET carbon-based nanocomposites

Ionizing radiation produces various reactive species in irradiated matter with free radicals and ions being the most important. Free radicals lead to chain reactions resulting either in crosslinking and/or degradation. The structure of the polymer chain and linear energy transfer (LET) of radiation are the most important factors that determine the impact on the solid polymer. Chemical bonds are formed in case the free radicals react by termination. If the radicals are on separate polymer chains, then crosslinking results. Other sequences of reactions lead to chain scission, formation of double bonds, or oxidation, if irradiation is performed in the presence of air. Degradation occurs if the polymer consists of saturated (single) carbon–carbon bonds or heteroatoms are present in the main polymer chain. Crosslinking results if unsaturated bonds (double, triple carbon–carbon bonds) are present. Although PET belongs to the first group of polymers, the presence of aromatic rings greatly improves its radiation stability.

Radiation-induced chain scission and crosslinking produce changes in the polymer chemical bonding, crystallinity, and molecular weight. The amorphous phase of semicrystalline polymers like PET is more radiation sensitive than the crystalline phase. Breaking of bonds and formation of shorter polymer chains may ease crystallization and increase the overall crystallinity while crosslinks present an obstacle to crystallization. Although the crystalline phase is less sensitive to radiation, the breaking of bonds and the rearrangement of the polymer structure around the ion path results in lattice deformations along the path of the ion. As a result, crystallinity is disturbed, and the quality of crystallites decreases.

The projected range of a 3-MeV proton beam in PET was calculated to be 112 μm using SRIM-2000 code. It was found that 99.94 % of the energy is lost due to electronic interactions [14]. It is of interest to monitor and compare the modifications of the physical–chemical

Table 2 The fraction of glycol segment in the *trans* conformation $\frac{I_{1340}}{I_{1410}}$, *gauche* conformation $\frac{I_{1370}}{I_{1410}}$ and the trans-gauche fraction for all the samples $\frac{I_{1340}}{I_{1370}}$, pristine *D0*, and proton irradiated under *D1*, *D2*, *D3* fluence condtions

	PET			PET–ND			PET–ND–NGP			
	D0	*D1*	*D2*	*D0*	*D1*	*D2*	*D0*	*D1*	*D2*	*D3*
$\frac{I_{1340}}{I_{1370}}$	0.330	0.760	1.080	0.360	3.188	6.010	0.360	0.380	6.260	6.460
$\frac{I_{1340}}{I_{1410}}$	0.139	0.305	0.566	0.150	0.724	1.024	0.153	0.181	0.892	1.111
$\frac{I_{1370}}{I_{1410}}$	0.422	0.396	0.523	0.420	0.227	0.170	0.428	0.453	0.146	0.172

properties of PET and PET nanocomposites exposed to high-energy radiation. FTIR spectra for proton-irradiated PET samples at different fluences along with the spectra for the unirradiated sample have been compiled into composite graphs for ease of comparison. Figure 2 shows the FTIR spectra in the region from 600 to 1800 cm^{-1} (a), and from 2600 to 3200 cm^{-1} (b), the regions of interest, of the nonirradiated PET sample and PET samples with successively higher proton irradiations. Spectra noted as *D1* are the spectra of PET samples irradiated with the fluence of 10^{14} p cm^{-2}, *D2*—10^{15} p cm^{-2} and *D3*—10^{16} p cm^{-2}.

At a proton fluence of 10^{14} p cm^{-2}, all of the characteristic vibrational bands were preserved except changes in intensity in the spectra were observed. This indicates that the overall polymer structure remains unchanged. The result is consistent with the findings of Singh et al. [13] who reported that PET is resistant to radiation-induced damage at least up to a fluence of 10^{14} p cm^{-2}. However, with increasing fluence, *D2* and *D3*, significant changes in the structure of the pure PET polymer were observed. The further decrease in intensity and broadening of the bands suggest an evolution of the polymer toward a more disordered state and a change in the degree of crystallinity. Under the highest fluence (D3), all the vibrational bands almost completely disappear, indicating chain breaking and amorphization, while a new band at 1605 cm^{-1}, attributed to monosubstituted benzene, appears [40, 41]. These findings suggest very significant changes in the structure of PET at the highest fluence, 10^{16} p cm^{-2}, and consequently in material properties. Loss of crystallinity, amorphization. and degradation are prominent for pure PET at this fluence.

Figures 3 and 4 show for comparison the spectra of nonirradiated and irradiated nanocomposites of PET–ND and PET–ND–NGP under the three selected fluences.

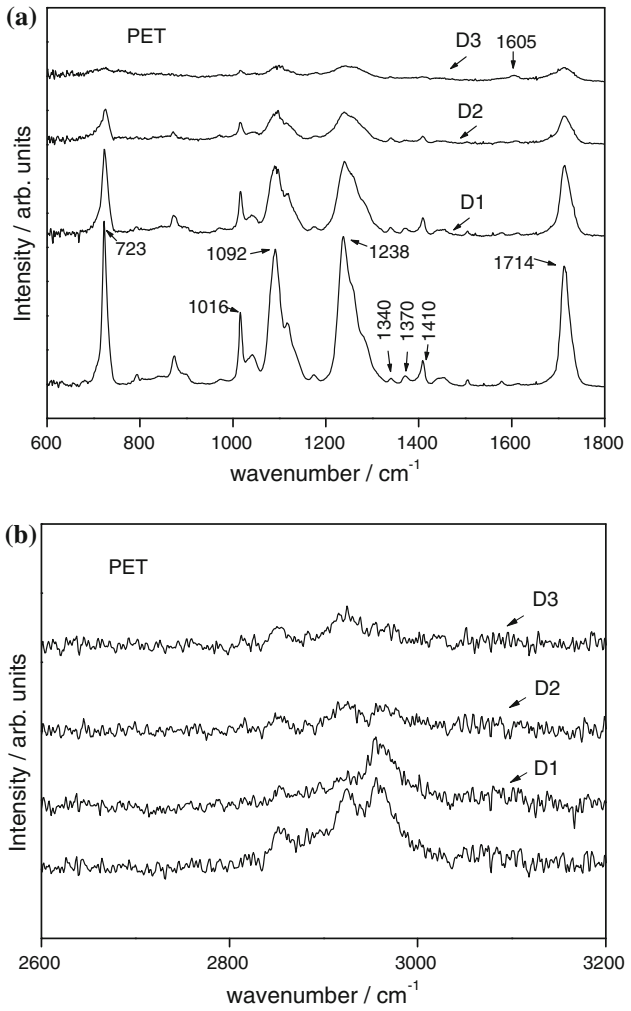

Fig. 2 PET FTIR spectra: **a** Pure PET nonirradiated (no label) and proton-irradiated PET to a fluence of *D1* 10^{14} p cm^{-2}; *D2* 10^{15} p cm^{-2}; *D3* 10^{16} p cm^{-2}: in region **a** 600–1800 cm^{-1} and **b** in region 2600–3200 cm^{-1}

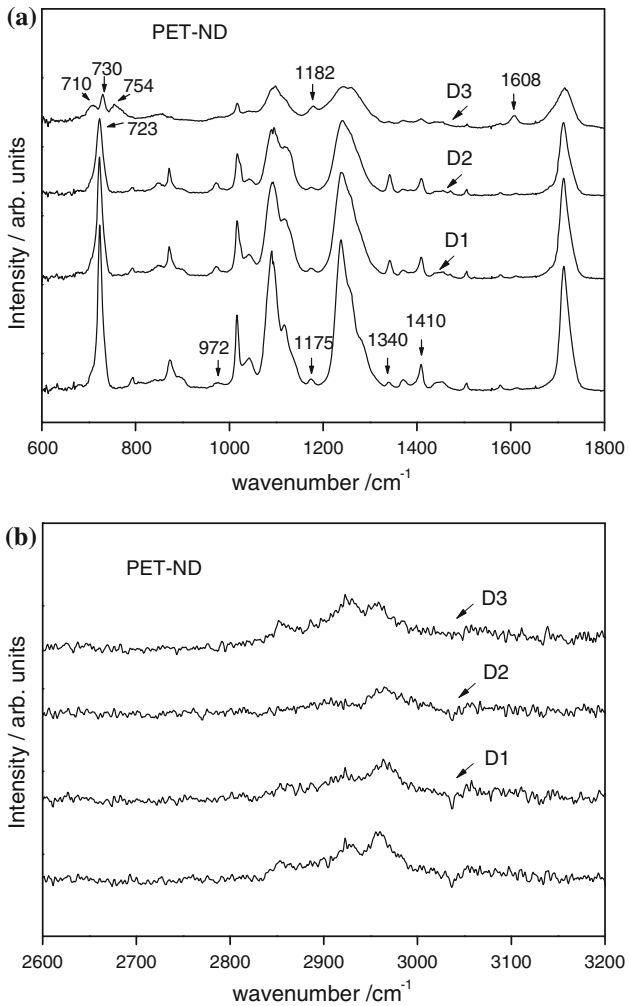

Fig. 3 FTIR spectra of PET–ND nanocomposites before and after irradiation. **a** Pure PET–ND nonirradiated (no label) and proton-irradiated PET–ND to a fluence of *D1* 10^{14} p cm^{-2}; *D2* 10^{15} p cm^{-2}; *D3* 10^{16} p cm^{-2}: in region **a** 600–1800 cm^{-1} and **b** in region 2600–3200 cm^{-1}

PET–ND nanocomposite (Fig. 3) and pure PET (Fig. 2) clearly show different behaviors under exposure to high-energy proton irradiation.

It is obvious that the decrease in the intensity of vibrational bands following irradiation is lower in the nanocomposites than in pure PET. While the intensity of the main vibrational bands in pure PET decreased almost in half with every next higher step in proton fluence, that tendency was suppressed in both nanocomposites, especially in the case of the PET–ND–NGP nanocomposite. Moreover, it can be seen in Fig. 3 that the absorption bands of the *gauche* conformations at 1370 cm^{-1}, *trans* conformations at 1340 cm^{-1} and the band at 1410 cm^{-1} show interesting and different behavior than in irradiated pure PET. It is obvious (Fig. 3) that the *gauche* conformation band decreased with the increasing fluence, while at the same time, the *trans* conformation band increased in intensity. The intensity of the band at 1410 cm^{-1} also did not change as much as in pure PET (see Fig. 2). The band at 874 cm^{-1}, attributed to the C–H out-of-plane deformation of the benzene ring in the terephthalate group, was almost unchanged for samples irradiated to fluences *D1* and *D2*, while the band at 975 cm^{-1} attributed to the *trans* C–H out-of-plane bending became more prominent with higher fluence.

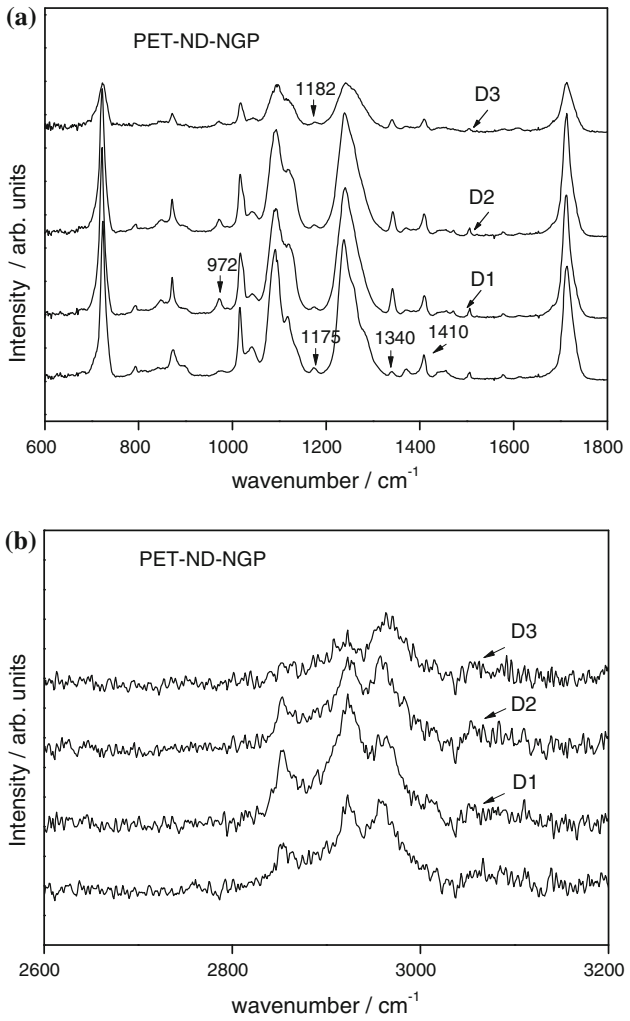

Fig. 4 PET–ND–NGP nanocomposite FTIR spectra before and after irradiation. **a** Pure PET–ND–NGP nonirradiated (no label) and proton-irradiated PET–ND–NGP to a fluence of *D1*, *D2*, and *D3* in region **a** 600–1800 cm^{-1} and **b** in region 2600–3200 cm^{-1}

Both bands are attributed to the *trans* conformation of the CH_2 groups in the crystalline (or ordered amorphous)-phase regions in PET. Furthermore, the shift of the ring band from 1175 cm^{-1} in PET–ND to 1182 cm^{-1} showed a planar conformation of the ring—ester segment characteristic of a crystalline phase. Similar behavior was observed for the PET–ND–NGP nanocomposite (Fig. 4), supporting the trend toward increased ordering in nanocomposite materials under proton irradiation for fluences as high as 10^{15}–10^{16} cm^{-1} (for PET–ND–NGP).

These findings suggest an increase in crystallinity in the region irradiated with 3 MeV protons for nanocomposite PET–ND, while the same was not so evident in the case of pure PET. In the case of the nanocomposite, it is still possible to clearly recognize all of the main vibrational bands even at the highest fluence, although the bands are less intense and broader. It is an indication that the presence of the nanoparticles increased the material tolerance toward proton irradiation. The new vibrational band at 1605 cm^{-1} attributed to monosubstituted benzene appeared, while the band at 723 cm^{-1} split into three 710, 730, and 754 cm^{-1}. Since the band at 730 cm^{-1} is assigned [40, 41] to out-of-plane bending of the benzene ring, and the band at 754 cm^{-1} band to benzene ring vibrations, the splitting may be associated with differences in the force field between amorphous and crystalline regions and also with the chain conformation around the glycol ester configuration. However, when subjected to the highest fluence the bands at 1410 and 1340 cm^{-1} are starting to disappear, indicating changes in the surrounding ring and possible carbonization.

FTIR spectra of nonirradiated and proton-irradiated PET–ND–NGP nanocomposite samples are presented in Fig. 4. A comparison of the spectra of the samples irradiated to fluences *D1* and *D2* versus the nonirradiated sample show almost unchanged characteristic vibrational bands. The intensities and the peak positions for the strongest PET bands at 1714 and 1238 cm^{-1} (stretching vibration in the ester linkage) and 723 cm^{-1} (CC in-plane bend ring and CH out-of-plane bend, ring) are almost the same as for the nonirradiated sample. The band at 795 cm^{-1} (CH out-of-plane bend, ring) is stable under fluences *D1* and *D2* as well as *D3*. The 1092 cm^{-1} band (CH in-plane bend plus C–O stretching) slightly decreased for *D2*. As illustrated in Fig. 4, vibrational bands at 975 and 1340 cm^{-1} attributed to the *trans* conformation of the CH_2 groups in the

crystalline region increase in intensity with the increasing fluence, while the intensity of the peak at 1370 cm^{-1} (*gauche* conformation attributed to the amorphous phase) decreases.

Even in the spectra of the nanocomposites irradiated to the highest fluence, *D3*, all the main characteristic bands of PET are still present with no changes in peak position. The intensity of the bands decreased although bands attributed to the *trans* conformation are still visible. This implies that proton irradiation caused additional crystallization of the starting material. The vibrational bands at 1605 cm^{-1} and splitting of the line at 723 cm^{-1} that were observed for the PET–ND nanocomposite were not detected in the spectra of the PET–ND–NGP nanocomposite. The PET–ND–NGP nanocomposite showed the highest degree of irradiation resistivity compared to pure PET and the PET–ND composite.

Previous analysis of the PET and PET nanocomposites spectra has shown the evolution of the *trans* conformation with incorporation of nanostructures for nonirradiated samples (Table 2). To compare the spectra of irradiated samples, we fit the vibrational bands in the frequency region (1300–1450 cm^{-1}) of pristine PET and the PET nanocomposites to a Lorentz shape. The fractions of glycol segments in *trans* and gauche conformations in pristine and irradiated PET, PET–ND, and PET–ND–NGP nanocomposites are tabulated in Table 2. Analysis of the fractions provide evidence of the development of the *trans* conformation under *D1* and *D2* irradiation even in pure PET. The progressive intensity increase of the band at 1340 cm^{-1}, due to the *trans* glycol conformation, and the corresponding decrease of the band at 1370 cm^{-1}, due to the *gauche* conformation, suggest the conversion of *gauche* into *trans* conformations as a result of proton irradiation. For samples irradiated to the fluence D3, the analysis was possible just for the the PET–ND–NGP nanocomposite where the absorptions bands corresponding to the presence of the *trans* and *gauche* conformations are still measurable. The evolution may also be connected with increased crystallinity or development of a more-ordered phase in irradiated samples.

The intensity of the band at 1410 cm^{-1} also changed as a result of proton irradiation. At fluence *D2*, the band intensity decreased for pure PET by 69 %, for PET–ND by 36 % and for PET–ND–NGP by 19 %. These trends suggest that the presence of the nanofillers may aid in preserving the ring structure. The process appears especially favored in the case of the PET–ND–NGP nanocomposite, which seems reasonable as the nanographene platelets have a similar ring structure as the starting PET polymer. The good thermal conductivity of graphene may contribute toward nanocomposite stability. Both ND and NGP may also act as traps/sinks for radiation-generated defects and free radicals helping to stabilize the polymer under high-energy/fluence irradiation.

Raman analysis

Recently, we have reported and discussed in detail the Raman spectra, as well as thermal and mechanical properties, of all pristine samples [42]. In this section, we present the analysis of Raman spectra of proton-irradiated samples in Fig. 5. It should be noted that the interpretation of the Raman spectra was only possible for the samples irradiated to the fluence *D1* or *D2* due to generation of irradiation-induced fluorescence (background). In the case of the *D2* fluence, the Raman spectra of PET–ND and PET–ND–NGP were observed. PET irradiated to the fluence *D2* as well as PET–ND irradiated to the fluence *D1* showed a high background, overwhelming the Raman signal. The appearance of strong photoluminescence (PL) following irradiation was reported previously for nanodiamond and nanodiamond-based nanocomposites [24].

In the Raman spectrum of PET, the bands centered at 633 and 1615 cm^{-1} have been related to ring vibration modes. The normal mode at 633 cm^{-1} is CCC in-plane ring bending, while the very strong band at 1615 cm^{-1} is connected to C=C ring stretching vibrations. The Raman band at 1730 cm^{-1} is related to the C=O stretching mode. Proton irradiation of PET to the fluence *D1* causes changes in intensities of ring vibration modes (scission of rings), whereas the intensity of the carbonyl stretching bond only slightly decreased. Further, the band at 1730 shifts to 1724 cm^{-1} due to changes in conformation of C=O groups which we associate with crystallization of terephthalate segments [42].

In the case of PET–ND, the Raman spectrum before and after irradiation exhibits a higher background. Yet it was still possible to recognize the decrease in the intensity of the 1615 band in comparison to the 1730 cm^{-1} band, showing that even in this sample, high-energy proton irradiation (*D2*) causes some ring scission.

However, it can be recognized from the PET–ND–NGP Raman spectra that the intensities of the bands remain the same under the *D1* fluence. Just for that sample, it was observed that even the *D2* fluence does not change significantly the intensities of the characteristic bands.

So, Raman analysis supports the FTIR finding that the addition of ND/NGP fillers preserves the polymeric structure of PET during high-energy proton irradiation.

DSC thermal analysis

Thermal analysis was conducted since it provides additional data on polymer properties, particularly semicrystalline polymers like PET. Changes in temperature and

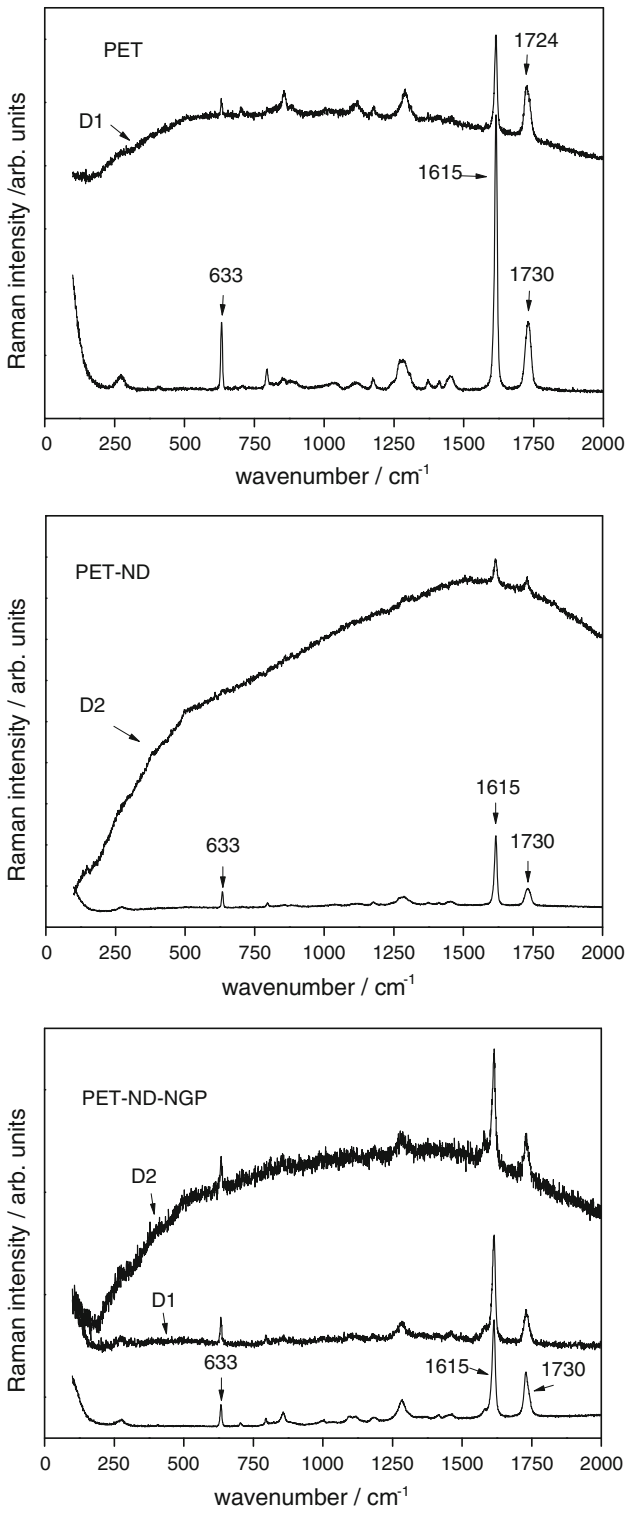

Fig. 5 Pure PET (*top*), PET–ND (*middle*) and PET–ND–NGP nanocomposite Raman spectra (*bottom*) before and after irradiation in the wavenumber region of 50–2000 cm^{-1}

heats of transformation arise due to structural changes in the polymer and the heat of melting is proportional to the degree of crystallinity.

DSC tests were performed to reveal differences in the thermal behavior between pristine and irradiated PET and PET nanocomposites as well as to gain information about the irradiation-induced changes in the crystallinity of the materials. To distinguish the effects of incorporating different carbon-based nanofillers into the PET matrix from those of proton irradiation, thermal analyses of the pristine PET polymer and of nonirradiated nanocomposite samples were performed under the same experimental conditions. DSC tests were performed on virgin, nonirradiated samples and just for irradiated regions *D1* and *D3* (irradiated regions of the samples were cut out from the rest of the sample).

DSC analysis for pristine PET, nanodiamonds, and graphene PET nanocomposites

DSC thermograms of the first heating, the first cooling and the second heating of pristine nonirradiated PET and PET–ND nanocomposites are presented in Fig. 6. All the data on transformation heats and temperatures are listed in Table 3. In all thermograms of the first heating (Fig. 6, top), three transformations can be seen: glass transition, T_g, at about 70 °C, cold crystallization, T_{cc} at about 130 °C and melting, T_m at about 245 °C. In semi-crystalline polymers, cold crystallization is an exothermic process of crystallization that for various reasons does not occur during the cooling from the melt [43]. The part of the amorphous phase that crystallizes is mostly the ordered amorphous phase also called the rigid amorphous phase (RAF) [44]. The ordered amorphous phase appears because the arrangement of long polymer chains and crystal formation upon cooling is hampered by the increasing viscosity of the cooling melt. As a result, parts of the same polymer chain may be included in both the crystalline and amorphous phases. Such molecules are called tie molecules because they connect amorphous and crystalline phases and form an interface with lower entropy than the rest of the amorphous phase. The dimensions of the ordered amorphous phase are such that it can be considered to be a nanophase. The ordered amorphous phase is prominent in polymers that contain rigid chain segments, like benzene rings in PET. Inefficient nucleation and/or spatial restraints to chain folding may also contribute. As a result, polymers like PET in fact have three phases: crystalline, ordered amorphous, and mobile amorphous phases as was already mentioned. This multiple phase composition results in specific thermal behavior and broadly influences all the polymer properties.

Upon heating above the glass transition temperature, the molecules trapped in the ordered amorphous phase attain enough energy to crystallize but the resulting crystals are of lower quality than those produced by the initial crystallization from the melt. Further heating causes complete

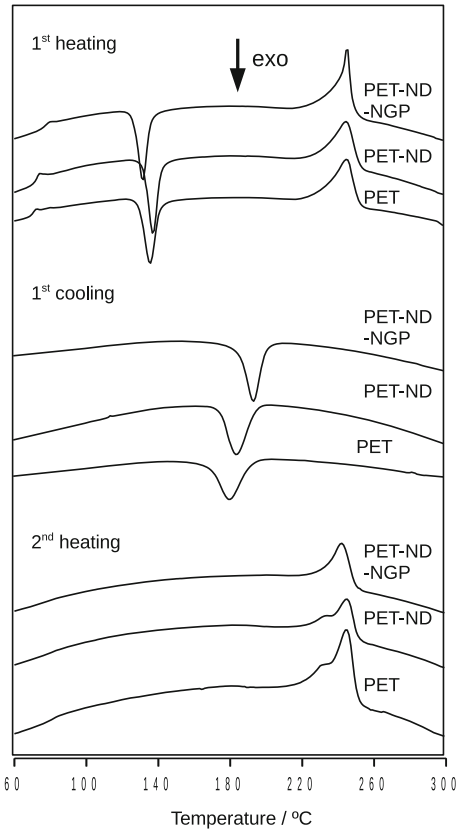

Fig. 6 DSC thermograms (normalized by mass) of nonirradiated PET and its PET–ND and PET–ND–NGP nanocomposites: *top* first heating, *middle* first cooling, and *bottom* second heating

fusion of the crystals previously formed upon cooling of the melt and of those resulting from cold crystallization. The fusion peak of the first heating of most samples, especially the nonirradiated samples, is simple, more or less sharp and without shoulders.

Only a single transformation is observed upon cooling of all studied PET and nanocomposite samples—crystallization. The thermograms of the first cooling are shown in the middle of Fig. 6; those of the second cooling are not shown since they are almost identical. No shoulders were observed in the crystallization peaks of any of the samples. The thermograms for all samples in the second heating (Fig. 6, bottom) display a hardly detectable glass transition, no cold crystallization peak, and a melting peak with a low-temperature shoulder; with the exception of the graphene-containing nanocomposite. The complex melting peaks appear because of the process of melting and recrystallization of the vitrified rigid amorphous phase that overlaps with the melting of the "true" crystalline phase. Some authors treat such complex melting in PET as melting/recrystallization/remelting [18, 45]. At relatively high cooling rates for PET and its nanocomposites, the segment of the amorphous phase that would otherwise form an ordered amorphous phase seems to have vitrified. As Righetti et al. [46] recently proposed, the vitrified RAF recrystallized upon heating, producing a more complex melting peak. At a slower cooling rate, the said segment of the amorphous phase probably would not have vitrified and most likely would have produced a cold crystallization peak upon reheating.

The temperatures of the cold crystallization and crystallization were more influenced by the addition of nanoparticles to PET than the glass transition and the melting temperatures. The glass transition temperature increase is possibly associated with the greater rigidity of the polymer due to interactions of functionalized nanodiamonds with the PET matrix. In the nanodiamond-only sample, PET–ND, both the glass transition and cold crystallization temperatures are higher than those in pristine PET. The increase in the cold crystallization temperature was not expected since increased nucleation by nanoparticles should have improved the initial crystallization and reduced the cold crystallization temperature. The increase indicates the presence of some obstacle to crystallization, such as crosslinking. Bikiaris et al. [47] studied PET–nanosilica nanocomposites and proposed that interactions between nanoparticles and the PET matrix result in a kind of physical network. They also observed a shift of cold crystallization to higher temperature. The slight increase of cold crystallization in the nanodiamond-only sample is consistent with the proposed interactions and, it also suggests an increased amount of ordered amorphous phase as a result of those interactions. The nucleating action of nanodiamonds is evident due to an increase in the crystallization temperature of the PET–ND nanocomposite (cooling cycle, Fig. 6b) compared to that of pure PET. Interactions between nanoparticles and the PET matrix did not influence the properties of the molten nanocomposite; however, upon solidification of the nanocomposite, those interactions become an obstacle to nucleation. As a result, the ordered amorphous phase becomes more stable so that, upon the second heating, the low-temperature shoulder in PET–ND is shifted to a higher temperature than that in pure PET.

The glass transition temperature of PET–ND–NGP is higher than that of the pure PET, while the cold crystallization temperature is lower which is consistent with the nucleation effect. Although the total concentration of nanoparticles is higher than that in the nanodiamond-only sample, the pronounced nucleation can be ascribed primarily to graphene which may have eased the crystallization of the ordered amorphous phase. The similarity between the graphene structure and the aromatic ring of the PET chain improves the quality of crystals formed from the ordered amorphous phase upon either cold crystallization or crystallization from the melt; as a result, all melting peaks in the PET–ND–NGP thermograms are sharp with no shoulders.

Table 3 Temperatures and heats of transformation of nonirradiated and irradiated PET and its nanocomposites determined by DSC

	D0			*D1*			*D3*		
	PET	PET–ND	PET–ND–NGP	PET	PET–ND	PET–ND–NGP	PET	PET–ND	PET–ND–NGP
1st heating									
T_g	70.3	72.0	74.6	72.0	72.0	72.0	73.0	72.1	74.2
T_{cc} (°C)	136.4	137.7	132.9	137.4	138.2	132.9	137.8	135.8	132.4
T_{cc} FWHM (°C)	6.3	5.7	5.6	6.2	7.0	6.4	10.9	6.9	6.2
Delta H_{cc} (J g^{-1})	−27.5	−28.2	−26.2	−12.7	−6.2	−8.4	−18.1	−4.2	−5.5
Shoulder T_{m1} (°C)				247.8	251.2			197.7	
T_{m1} (°C)	244.8	246.5	246.7	241.4	244.6	243.0	237.4	244.4	245.5
T_{m1} FWHM (°C)	13.3	12.9	9.4	19.3	23.8	17.8	20.8	13.2	10.2
Delta H_{m1} (J g^{-1})	41.6	39.6	43.3	36.5	28.1	37.5	40.9	17.2	25.0
1st cooling									
T_{c1} (°C)	178.3	185.0	204.8	181.8	190.4	207.0	186.0	199.1	210.6
T_{c1} FWHM (°C)	14.4	11.7	8.3	14.2	16.6	13.4	11.8	9.6	7.7
Delta H_{c1} (J g^{-1})	−29.9	−32.8	−33.9	−13.1	−18.5	−25.7	−9.1	−15.7	−15.7
2nd heating									
Shoulder T_{m2} (°C)	227.3	232.5			245.7			237.4	
T_{m2} (°C)	243.7	245.7	242.7	240.9	243.9	241.8	235.0	244.4	243.0
T_{m2} FWHM (°C)	12.5	13.1	11.6	17.4	25.8	16.3	18.1	18.7	10.8
Delta H_{m2} (J g^{-1})	32.2	42.4	35.5	36.7	21.1	29.1	40.1	18.0	22.7
2nd cooling									
T_{c2} (°C)	174.4	183.5	204.0	179.9	191.9	207.5	186.0	200.8	211.9
T_{c2} FWHM (°C)	18.0	12.2	8.4	14.1	16.4	14.0	10.6	8.9	7.7
Delta H_{c2} (J g^{-1})	−24.2	−34.3	−34.0	−11.0	−17.9	−28.3	−6.5	−16.7	−16.3

The full-width at half-maximum (FWHM) is an indicator of the uniformity of the crystallizing chains. The FWHM of the first crystallization peak is significantly lower in the PET–ND–NGP nanocomposite than in PET or PET–ND nanocomposite indicating that graphene might also improve the quality of the crystalline phase. Polymer chains more or less lose their orientation in molten PET. Similar to the orienting effects of SWNT proposed by Anoop et al. [48], the NGP may provide a template that improves organization of the PET chains, improves crystallization, and reduces the number of defects that would otherwise contribute to formation of an ordered amorphous phase. The nucleating effect of NGP is also obvious upon crystallization from the melt, as the crystallization temperature is higher by more than 26 °C than that of PET and higher by almost 20 °C than that of the PET–ND nanocomposite.

Heats of melting are not significantly influenced by the addition of nanoparticles, particularly upon the first heating, indicating that the overall crystallinity is not significantly affected. The heats of crystallization of nanocomposites are greater than that of pure PET. The PET–ND nanocomposite has an intermediate heat of crystallization.

DSC analysis of proton-irradiated PET and PET carbon-based nanocomposites

Changes in the thermal properties of pristine PET and its nanocomposites produced by proton irradiation can be observed in partial DSC thermograms in Fig. 7 and in corresponding transformation temperatures and heats listed in Table 3. Heats of the most of the transformations generally decreased with increasing fluence. In some samples, local microscopic carbonization appeared at the highest fluence, D3, indicating decomposition of the PET matrix. Still, complete amorphization in PET and its nanocomposites was never achieved which is likely due to the higher radiation stability of the crystalline phase of the PET matrix (to which added nanostructures contribute).

In irradiated samples, the glass transition and cold crystallization temperatures shifted indicating that the majority of the changes occurred in the amorphous phase(s).

The glass transition temperatures of irradiated samples (Table 3) of pure PET slightly increased with fluence, while it was almost unchanged in the PET–ND nanocomposite. T_g in the PET–ND–NGP nanocomposite is slightly lower at D1 but increases upon irradiation to the D3 fluence to become almost the same as that for the nonirradiated PET–ND–NGP nanocomposite. An increase in the glass transition temperatures indicates an increase in overall rigidity that is most likely caused by secondary radiation-induced crystallization (SRIC) [49, 50] of short polymer chains formed by breaking the bondage of PET macromolecules. The SRIC also causes a decrease in heats of cold crystallization, while corresponding temperatures varied. The T_{cc} of pure PET and PET–ND nanocomposites slightly increased with fluence, but that of PET–ND–NGP nanocomposite remained almost unchanged. The increased rigidity of the amorphous phase and higher cold crystallization temperatures may also result from a low extent of crosslinking because of free radical termination. The concentrations of those new C–C bonds that influenced the T_g temperature in DSC thermograms are likely too low to be observed in FTIR spectra. Since both glass transition and cold crystallization temperatures are almost unchanged in irradiated PET–ND–NGP nanocomposites, it can be concluded that graphene decreased the radiation sensitivity of the amorphous phase. For the irradiated graphene-containing nanocomposite, some radiation damage is observed only at the *D3* fluence, since its cold crystallization peak has a high-temperature shoulder. Zhu et al. [43] ascribed such a shoulder to an interspherulitic amorphous phase, while the main cold crystallization peak is a result of an interlamellar amorphous phase.

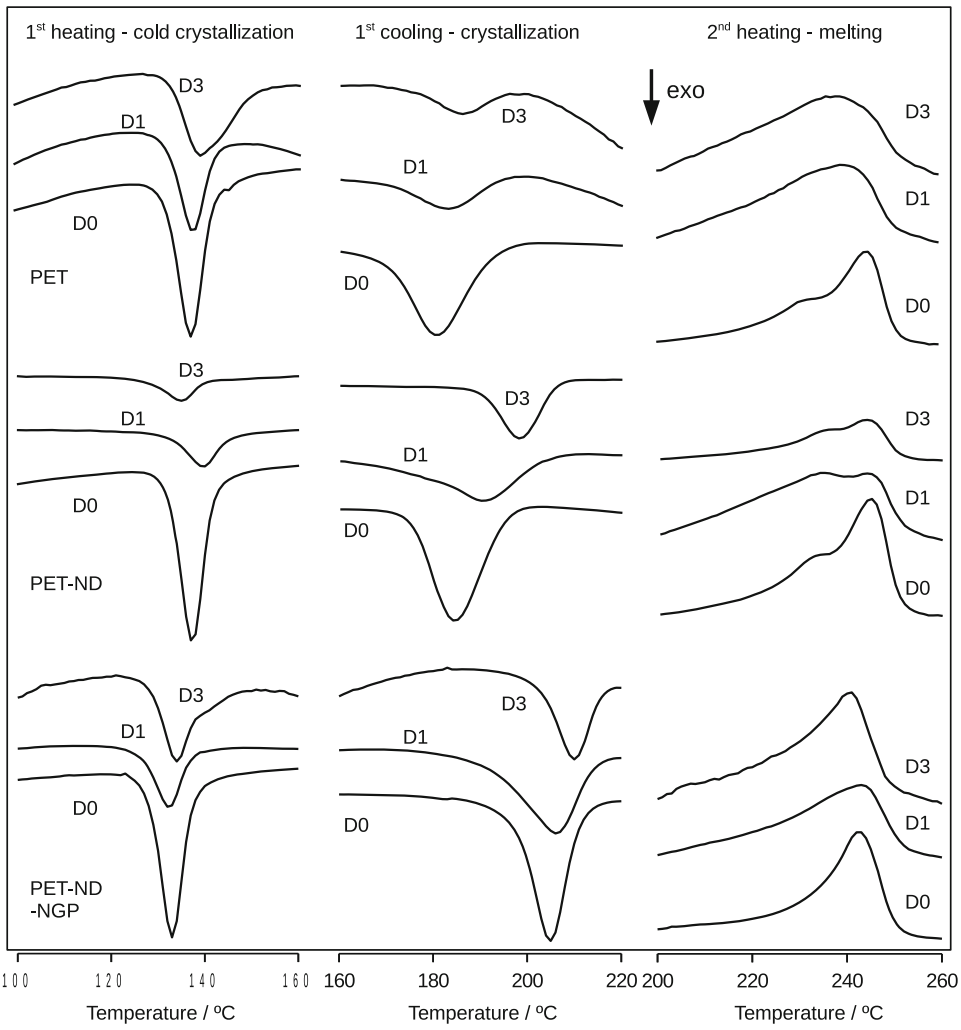

Fig. 7 Details of DSC thermograms (normalized by mass) of nonirradiated and irradiated samples: 1st row pure PET, 2nd row PET–ND nanocomposite, and 3rd row PET–ND–NGP nanocomposite; *left* cold crystallization (first heating), *middle* crystallization on the first cooling, and *right* melting on the second heating

The peak melting temperature, T_m, of polymers increases with molecular mass up to a certain threshold value, above which it becomes constant. A decrease in the melting temperature in irradiated samples would indicate significant depolymerization as observed, e.g., by Liu et al. [51] in particle-irradiated PET samples. In our PET and its nanocomposites, the maximum peak temperature of melting did not change significantly probably because of lower LET of protons compared to the ions Liu et al. [51] used. Therefore, since the melting temperatures are not much lower decomposition of the PET matrix can be excluded under the conditions of these experiments. Still the melting peaks became wider and had poorly defined boundaries with the exception of peaks in the PET–ND–NGP nanocomposite. Such behavior indicates that the proton irradiation influenced recrystallization and remelting of the ordered amorphous phase and confirms that the amorphous phase is more affected than the crystalline phase. An apparent increase in the heats of melting, which was observed for irradiated pure PET, is at least in part caused by the contribution of SRIC. Other factors may also be partly responsible for broadening of the peaks of melting. Any radiation-induced chemical reactions in the PET matrix (crosslinking, degradation. and branching) widens the molecular mass distribution, thus broadening the melting peak and resulting in increased FWHM values of melting peaks of first heating of irradiated PET and PET–ND nanocomposite with increasing fluence. At the same time, the integration boundaries became obscured, particularly in PET and PET–ND nanocomposites. In PET–ND, interactions between nanodiamonds and the PET matrix seem to stabilize the remaining crystalline phase, so the shoulder that appears upon the second heating even shifted to a higher temperature, particularly at *D1*. Only in the irradiated PET–ND–NGP nanocomposite did the melting temperatures remain almost constant and the melting peaks remained defined, although less so at the highest fluence. The FWHM values of PET–ND–NGP nanocomposite melting peaks are also the lowest, indicating better quality crystallites in nonirradiated samples that are less affected by irradiation.

Defects introduced into the samples by irradiation, irrespective of their type, act as nucleation sites, so the number of crystallites increased but their quality was lower causing a shift of the peak crystallization-from-the-melt temperature, T_{c1} or T_{c2} to higher values. This behavior is most pronounced in PET–ND nanocomposites. T_{c1} and T_{c2} temperatures of irradiated samples also increased with fluence, and the change is the most pronounced in PET–ND nanocomposites. Since the FWHM of the crystallization peaks of PET–ND nanocomposites also increased, it indicates that short chains were formed by the degradation of the polymer matrix, and those chains crystallize at somewhat higher temperature. Again, the crystallization temperatures are the highest with the lowest FWHM in irradiated PET–ND–NGP nanocomposites. The crystallization-from-the-melt temperature of PET–ND–NGP nanocomposite irradiated to the highest fluence, *D3*, is the highest of all the measured samples. The overall difference of the lowest (nonirradiated pure PET) and the highest temperature of crystallization from the melt (PET–ND–NGP nanocomposite at *D3* fluence) is almost 35 °C. Because of the complex structure of the PET melting peak, it is easier to assess the changes in crystallinity of irradiated PET and its nanocomposites from heats of crystallization. As already stated, under the conditions of these DSC experiments, the ordered amorphous phase segment vitrified upon cooling and did not contribute to the crystallization peak. All the crystallization heats decreased with fluence, but that of the PET–ND–NGP nanocomposite remained the highest up to *D3* fluence, indicating the highest radiation stability.dissapeared.

Photoluminescence studies

In the present study, proton beam-induced modifications of the photoluminescence behavior of the PET polymer and PET nanocomposites were evaluated. No luminescence was observed for any of the nonirradiated samples. This was expected as the intrinsic emission bands cannot be effectively stimulated by 405-nm photons.

However, following irradiation PL measurements revealed complicated features in the spectra. The PL spectra of pristine PET irradiated under *D1*, *D2* and *D3* fluence conditions are shown in Fig. 8. The emission spectra consists of several characteristic peaks in the wavelength range between 400 and 800 nm, with several different peaks around 500, 550, and 600 nm. No changes were found in the wavelength range higher than 800 nm. The results suggest that several different emission centers exist following 3 MeV proton irradiation.

Nagata et al. [52] reported radiation-induced luminescence of PET and PEN films (with 1 MeV H+, He). They also observed a decrease in PL intensity in the wavelength range between 400 and 600 nm. Our samples were irradiated at a higher energy and to a higher fluence (*D3*). The PL spectrum of the PET sample irradiated to the fluence *D1* has the highest intensity for the band in the 450–700-nm region (Fig. 8). The PL intensity decreased with increasing irradiation dose. At the *D3* fluence, the PL emission almost completely disappeared. The PL intensity is sensitive to defects introduced by proton irradiation. Therefore, the decrease in luminescence intensity with increasing irradiation dose might be attributed to the formation of defects and destruction/modification of the chemical structure due to the increase in the energy deposited by the proton beam

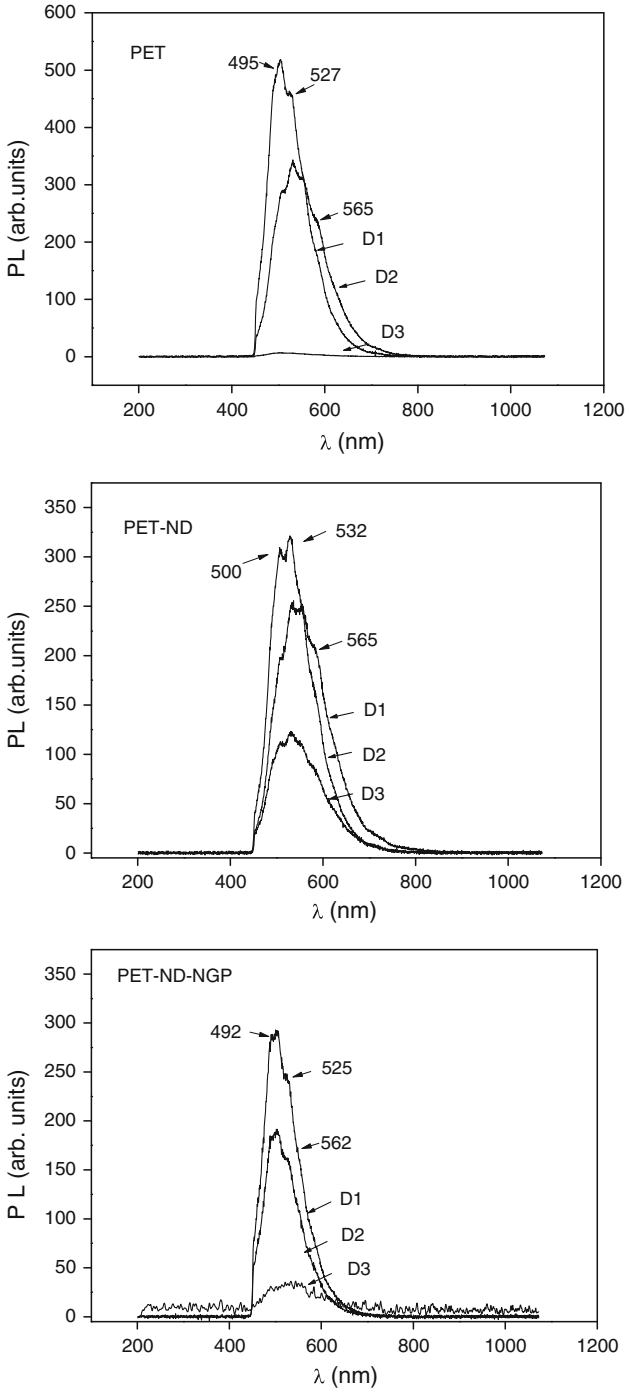

Fig. 8 PL spectra of PET irradiated under *D1*, *D2*, and *D3* conditions (*top*); PL spectra of PET–ND irradiated under *D1*, *D2*, and *D3* conditions (*middle*); and PL spectra of PET–ND–NGP irradiated under *D1*, *D2*, and *D3* conditions (*bottom*)

in the sample. With increasing irradiation dose, the polymer material becomes more enriched with defects, which affect the radiative transitions. The decrease in luminescence suggest the formation of new radiative recombination levels, which can be related to the irradiation-induced compositional transformation in the irradiated region. The emission peak at around 550 nm has been reported in other polymers [41] and hydrogenated carbon films and was related to aggregates of phenyl radicals. The PL emission which appears above 500 nm in the PET may be attributed to similar medium range ordered structures of carbon clusters.

The PL spectra of PET–ND and PET–ND–NGP nanocomposites subjected to *D1*, *D2*, and *D3* irradiation conditions are presented in Fig. 8 (middle and bottom). The highest PL intensity was again recorded for the *D1* irradiation condition in both PET–ND and PET–ND–NGP nanocomposites. However, the PL spectra for *D1* fluence conditions in both nanocomposites were less intense than the PL intensity for pure PET. Also, the same pattern of decreasing intensity with increasing proton irradiation dose was observed. However, the decrease was not as drastic as for pure PET. This indicates that the higher irradiation fluence did not introduce as many new radiative recombination levels, which can be related to irradiation-induced compositional transformation of the irradiated region as in the case of pure PET. These findings support the previous FTIR results of higher irradiation resistance of nanocomposite PET materials.

Conclusion

The ATR-FTIR, DSC, and Raman studies reveal that the introduction of ND and ND–NGP nanofillers did not significantly change the properties of the polymeric matrix and that only minimal differences in sample crystallinity existed between virgin samples and the nanocomposites. The proton irradiation at a fluence of 10^{14} p cm^{-2} (*D1*) caused minimal modifications to the polymer structure although the nanocomposites showed much less change in the vibrational bands intensities compared to those of pure PET. It was also shown, with both FTIR and DSC measurements, that for a fluence of 10^{14} p cm^{-2} all the materials gained some degree of crystallinity and became more ordered. This was explained by proton beam breaking of polymer chains, producing short segments that crystallize easier and therefore a slight increase in the degree of crystallinity was observed for all the samples. Further increase in fluence leads to more different reactions of the pure PET versus PET nanomaterials. It was shown that while pure PET becomes more degraded, the nanomaterials tend to retain all the vibrational bands, particularly PET–ND–NGP nanocomposite, with further increase in the *trans* conformation and decrease in *gauche* conformation, indicating further development of more ordered areas inside the amorphous material. Raman measurements confirmed that the intensity of the bands in PET–ND–NGP nanocomposite does not change significantly under *D1* and

D2 fluence, while proton irradiation of neat PET to the fluence *D1* introduced already the changes in intensities of ring vibration modes. The most significant difference in material response to proton irradiation in the case of the highest irradiation fluence *D3* (which in our study was 10^{16} p cm^{-2}) has been observed for the material with ND and NGPs fillers. While pure PET underwent almost complete amorphization, it was clearly shown that all the vibrational bands are still present in the nanocomposites, especially in the case of PET–ND–NGP nanocomposite, and the crystallization process or some degree of ordering occurred with the nanoparticles/nanoplatelets serving as nucleating agents. As a consequence the nanocomposites are less sensitive to proton irradiation than pure PET.

We showed that the presence of those nanomaterials lead to stabilization of the PET matrix; the degradation of the polymer is retarded by the presence of the nanoparticles which may restrict the thermal motion of PET molecules, serve as heat sinks, ease the crystallization process, block free radicals and thus increase thermal stability and radiation hardness. Furthermore, the materials underwent a change in optical emission properties following irradiation. Excitation with a 405-nm laser beam resulted in luminescence which was observed for all the samples while the luminescence was not present in nonirradiated material. With irradiation, PET became more enriched with defects which serve as emission centers that affect the radiative transitions. Higher irradiation fluence did not introduce so many new radiative recombination levels in the nanocomposites which can be related to irradiation-induced compositional transformation of the irradiated region. These findings support the FTIR results of higher irradiation resistance of nanocomposite PET materials.

The present investigation contributes toward a better understanding of the modifications of the structural, optical, and thermal properties of PET and its composite nanomaterials induced by proton beam irradiation which is applicable to the use of these materials in high radiation environments.

Compliance with ethical standards

Conflict of Interest The authors declare that they have no conflict of interest.

References

1. Jabarin SA (1996) Polymeric materials encyclopedia. CRC press, New York, pp 6078–6085, 6091–6100
2. Chandy T, Das GS, Wilson RF, Rao GHR (2000) Use of plasma glow for surface-engineering biomolecules to enhance blood compatibility of Dacron and PTFE vascular prosthesis. Biomaterials 21:699–712
3. Bisson I, Kosinski M, Ruault S, Gupta B, Hilborn J, Frey P (2002) Acrylic acid grafting and collagen immobilization on poly(ethylene terephthalate) surfaces for adherence and growth of human bladder smooth muscle cells. Biomaterials 23:3149–3158
4. Ravindranath K, Mashelkar RA (1986) Polyethylene terephthalate—I. Chemistry, thermodynamics and transport properties. Chem Eng Sci 41:2197–2214
5. Varma P, Lofgren EA, Jabarin SA (1998) Properties and kinetics of thermally crystallized orientated poly(ethylene terephthalate) (PET) I: kinetics of crystallization. Polym Eng Sci 38:237–244
6. Hanemann T, Szabó DV (2010) Polymer-nanoparticle composites: from synthesis to modern applications. Materials 3:3468–3517
7. Vaia RA, Wagner HD (2004) Framework for nanocomposites. Mater Today 7:32–37
8. Ray SS, Okamoto M (2003) Polymer/layered silicate nanocomposites: a review from preparation to processing. Prog Polym Sci 28:1539–1641
9. Carrado KA (2003) Polymer-clay nanocomposites. In: Shonaike GO, Advani SG (eds) Advanced polymeric materials: structure property relationships. CRC Press, Boca Raton, pp 349–396
10. Mishra R, Tripathy SP, Sinha D, Dwivedi KK, Ghosh S, Khathing DT, Muller M, Fink D, Chung WH (2000) Optical and electrical properties of some electron and proton irradiated polymers. Nucl Instrum Methods B 168:59–64
11. Bridwell LB, Giedd RE, Wang YQ, Mohite SS, Jahnke T (1991) Ion implantation of polymers for electrical conductivity enhancement. Nucl Instrum Methods B 56(57):656–659
12. Keiji U, Yasuyo M, Nobuyuki N, Mitsuru N, Mamoru S (1991) Effects of high-energy (MeV) ion implantation of polyester films. Nucl Instrum Methods B 59(60):1263–1266
13. Singh NL, Shah N, Desai CF, Singhb KP, Arora SK (2004) Modification of polyethylene terephthalate by proton irradiation. Radiat Eff Defect Solids 159:475–482
14. Singh NL, Shah N, Singh KP, Desai CF (2005) Electrical and thermal behavior of proton irradiated polymeric blends. Radiat Meas 40:741–745
15. Fink D (2004) Springer series in material science: fundamentals of ion-irradiated polymers. Springer, Berlin Heidelberg
16. Cury Camargo PH, Gundappa Satyanarayana K, Wypych F (2009) Nanocomposites: synthesis, structure, properties and new application opportunities. Mater Res 12:1–39
17. Kim JY, Kim SH (2012) High performance PET/carbon nanotube nanocomposites: preparation, characterization, properties and applications. In: Ebrahimi F (ed) Nanocomposites—new trends and developments. InTech, Chapter 5
18. Tzavalas S, Mouzakis DE, Drakonakis V, Gregoriou VG (2008) Polyethylene terephthalate–multiwall nanotubes nanocomposites: effect of nanotubes on the conformations, crystallinity and crystallization behavior of PET. J Polym Sci Part B 46:668–676
19. Liu Y, Kumar S (2014) Polymer/carbon nanotube nano composite fibers—a review. Appl Mater Interfaces 6:6069–6087
20. Wang C, Guo ZX, Fu S, Wu W, Zhu D (2004) Polymers containing fullerene or carbon nanotube structures. Prog Polym Sci 29:1079–1141
21. Mochalin VN, Shenderova O, Ho D, Gogotsi Y (2012) The properties and applications of nanodiamonds. Nat Nanotechnol 7:11–23
22. Borjanovic V, Bistricic L, Mikac L, McGuire GE, Zamboni I, Jaksic M, Shenderova O (2012) Poymer nanocomposites with improved resistance to ionizing radiation. J Vac Sci Technol, B 30:1023–1071
23. Borjanovic V, Bistricic L, Vlasov I, Furic K, Zamboni I, Jaksic M, Shenderova O (2009) Influence of proton irradiation on the structure and stability of poly(dimethylsiloxane) and poly(dimethylsiloxane)-nanodiamond composite. J Vac Sci Technol, B 27:2396–2403
24. Borjanovic V, Lawrence WG, Hens S, Jaksic M, Zamboni I, Edson C, Vlasov I, Shenderova O, McGuire GE (2008) Effect of

proton irradiation on photoluminescent properties of PDMS-nanodiamond composites. Nanotechnology 19:455701. doi:10.1088/0957-4484/19/45/455701
25. Borjanovic V, Shenderova O, McGuire GE (2013) Polymer nanocomposites with improved resistance to ionizing radiation, U.S. Patent No. 8, 475, 879
26. Galpaya D, Wang M, Liu M, Motta N, Waclawik E, Yan C (2012) Recent advances in fabrication and characterization of graphene-polymer nanocomposites. Graphene 1:30–49
27. Das TK, Prusty S (2013) Graphene-based polymer composites and their applications. Polym Plast Technol 52:319–331
28. Zhang HB, Zheng WG, Yana Q, Yang Y, Wang JW, Lu ZH, Ji GY, Yu ZZ (2010) Electrically conductive polyethylene terephthalate-graphene nanocomposites prepared by melt compounding. Polymer 51:1191–1196
29. Prasad KE, Das B, Maitra U, Upadrasta Ramamurty U, Rao CNR (2009) Extraordinary synergy in the mechanical properties of polymer matrix composites reinforced with 2 nanocarbons. Proc Natl Acad Sci USA 106:13186–13189
30. Shenderova S, Koscheev A, Zaripov N, Petrov I, Skryabin Y, Detkov P, Turner S, Van Tendeloo G (2011) Surface chemistry and properties of ozone-purified detonation nanodiamonds. J Phys Chem C 115:9827–9837
31. Chen Z, Hay JN, Jenkins MJ (2013) The thermal analysis of poly(ethylene terephthalate) by FTIR spectroscopy. Thermochim Acta 552:123–130
32. Chen Z, Hay JN, Jenkins MJ (2012) FTIR spectroscopic analysis of poly(ethylene terephthalate) on crystallization. Eur Polym J 48:1586–1610
33. Bertoldo M, Massimiliano Labardi M, Rotella C, Capaccioli S (2010) Enhanced crystallization kinetics in poly(ethylene terephthalate) thin films evidenced by infrared spectroscopy. Polymer 51:3660–3668
34. Rastogi R, Vellinga WP, Rastogi S, Schick C, Meijer HEH (2004) The three-phase structure and mechanical properties of poly(ethylene terephthalate). J Polym Sci Pol Phys 42:2092–2106
35. Cunningham A, Ward MI, Willis H, Zichy V (1974) An infra-red spectroscopic study of molecular orientation and conformational changes in poly(ethyleneterephthalate). Polymer 15:749–756
36. Schmidt PG (1963) Polyethylene terephthalate structural studies. J Polym Sci Part A 1:1271–1292
37. Jabarin SA (1982) Optical properties of thermally crystallized poly(ethylene terephthalate). Polym Eng Sci 22:815–820
38. Cole KC, Ajji A, Pellerin E (2002) New insights into the development of ordered structure in poly(ethylene terephthalate)—1. Results from external reflection infrared spectroscopy. Macromolecules 35:770–784
39. Kirov KR, Assender HE (2005) Quantitative ATR-IR analysis of anisotropic polymer films: surface structure of commercial PET. Macromolecules 38:9258–9265
40. Moeller HW (2008) Progress in polymer degradation and stability research. Nova Science Publishers, Inc, New York
41. Quaranta A, Vomiero A, Cartura S, Maggioni G, Mea GD (2002) Polymer film degradation under ion irradiation studied by ion beam induced luminescence (IBIL) and optical analyses. Nucl Instr Methods B 191:680–684
42. Bistricic L, Borjanovic V, Leskovac M, Mikac L, McGuire GE, Shenderova O, Nunn N (2015) Raman spectra, thermal and mechanical properties of poly(ethylene terephthalate) carbon based nanocomposite films. J Polym Res 22:39
43. Zhu P, Ma D (1997) Double cold crystallization peaks of poly(ethylene terephthalate)—1. Samples isothermally crystallized at low temperature. Eur Polym J 33:1817–1818
44. Androsch R, Wunderlich B (2005) The link between rigid amorphous fraction and crystal perfection in cold-crystallized poly(ethylene terephthalate). Polymer 46:12556–12566
45. Tzavalas S, Drakonakis V, Mouzakis DE, Fischer D, Gregoriou VG (2006) Effect of carboxy-functionalized multiwall nanotubes (MWNT-COOH) on the crystallization and chain conformations of poly(ethylene terephthalate) PET in PET-MWNT nanocomposites. Macromolecules 39:9150–9156
46. Righetti MC, Laus M, Di Lorenzo ML (2014) Rigid amorphous fraction and melting behavior of poly(ethylene terephthalate). Colloid Polym Sci 292:1365–1374
47. Bikiaris D, Vassilis K, Karayannidis G (2006) A new approach to prepare poly(ethylene terephthalate)/silica nanocomposites with increased molecular weight and fully adjustable branching or crosslinking by SSP. Macromol Rapid Commun 27:1199–1205
48. Anoop Anand K, Agarwal US, Rani J (2006) Carbon nanotubes induced crystallization of poly(ethylene terephthalate). Polymer 47:3976–3980
49. Biswas A, Lotha S, Fink D, Singh JP, Avasthi DK, Yadav BK, Bose SK, Khating DT, Avasthi AM (1999) The effects of swift heavy ion irradiation on the radiochemistry and melting characteristics of PET. Nucl Instr Methods B 159:40–51
50. Papaleo RM, de Araujo MA, Livi RP (1992) Study of the ion beam induced amorphisation, bond breaking and optical gap change processes in PET. Nucl Instr Methods B 65:442–446
51. Liu C, Jin Y, Sun Y, Hou M, Wang Z, Chen X, Zhang C, Liu J, Liu B, Wang Y (2000) Chemical modifications in polyethylene terephthalate films induced by 35 MeV/u Ar ions. Nucl Instr Methods B 166(167):641–645
52. Nagata S, Takahiro K, Tsuchiya B, Shikama T (2009) Ion beam induced luminescence of polyethylene terephthalate foils under MeV H and He ion bombardment. Nucl Instr Methods B 267:1553–1556